Long-cycling of a water-soluble quinizarin derivative in redox flow batteries: Role of the cut-off voltage on the stability

Ines Ozouf, Jean-Marie Fontmorin, Raphael Lebeuf, Gaël Mathieu, S. Guiheneuf, G. Ozouf, Véronique Rataj, T. Godet-Bar, Didier Floner, Jean-Marie Aubry, et al.

Long-cycling of a water-soluble quinizarin derivative in redox flow batteries: role of the cut-off voltage on the stability

I. Ozouf,[a] J.-M. Fontmorin,[a,c] R. Lebeuf,*[b] G. Mathieu,[a] S. Guiheneuf,[a,c] G. Ozouf,[c] V. Nardello-Rataj,[b] T. Godet-Bar,[c] D. Floner,[a] J.-M. Aubry,[b] F. Geneste*[a]

[a] Univ Rennes, CNRS, ISCR, UMR 6226, F-35000 Rennes, France

[b] Univ. Lille, CNRS, Centrale Lille Institut, ENSCL, Univ. Artois, UCCS, UMR 8181 F-59000 Lille, France

[c] Kemiwatt, 11 allée de Beaulieu CS 50837 F-35708 Rennes Cedex 7

Keywords : aqueous organic redox flow battery; quinizarin; stability; cut-off voltage; anthraquinone

Abstract

To improve the industrial applicability of aqueous organic redox flow batteries (AORFB), inexpensive redox compounds highly soluble in aqueous medium and stable during cycling are required. Thus, a water-soluble quinizarin derivative, 1,4-dihydroxy-2-carboxymethyl-9,10-anthraquinone (1,4-CDHAQ) prepared by a one-pot synthesis from relatively low-cost leucoquinizarin (widely used as intermediate in the dye industry) is evaluated in AORFB. It exhibits a good solubility in basic medium (> 0.4 M) and a low potential (-0.64 V *vs* Ag/AgCl) leading to a cell voltage of about 1 V when paired with ferri/ferrocyanide couple. Long-cycling AORFB of 2.5 months performed at a concentration of 0.4 M gives good performance in terms of energy efficiency and power density. The influence of the temperature on ASR values and so on the power density underlines the difficulty to obtain reproducible results at room

temperature. A capacity fade rate of 0.008%/cycle (0.28%/day) is obtained after 2500 cycles, which is close to other values reported for anthraquinones in strong basic medium for long-cycling tests. Interestingly, the discharge cut-off voltage clearly affects the stability of the battery, leading to the formation of different degradation products as shown by ^{1}H-NMR. These results highlight the importance of the cycling conditions to improve the battery performance.

1. Introduction

The development of renewable energies such as wind and solar photovoltaics requires efficient, low-cost and scalable stationary energy storage systems. Redox flow battery is a promising technology with a flexible and simple design decoupling power (Watt) and energy (Watt-hour) and giving rise to reliable long-term performance. Aqueous organic redox flow batteries (AORFBs) have been widely investigated as they have many advantages [1-5]. Molecular engineering uses organic elements that are abundant on earth and offers tremendous possibilities for improving performance in terms of safety, cost, solubility, redox potential, kinetics and stability. Moreover, despite its rather narrow electrochemical potential window, water is a very efficient solvent because it is cheap, extremely safe and highly conductive. Although viable industrial systems arrive on the market (CMBlu, JenaBatteries, Kemiwatt, Lockheed Martin, Quinoenergy, etc.), some technological barriers must be overcome for further development to reach requirements in terms of energy and power density, and stability. Among all organic molecules that are electroactive in aqueous medium, quinones are the most studied [2, 6]. In particular, anthraquinone derivatives have attracted much attention owing to their high chemical stability, high molecular mass limiting crossover, molecular diversity and to the possibility to be used in acidic, neutral and basic medium [7]. Alkaline solutions are particularly interesting since in such media, the nontoxic ferri/ferrocyanide redox couple can be used as

posolyte [8-10]. Commercially available hydroxyanthraquinones such as 1,4-dihydroxyanthraquinone (quinizarin), 1,2-dihydroxyanthraquinone (alizarin) and 2,6-dihydroxyanthraquinone (anthraflavic acid) present interesting properties in basic solutions due to the presence of phenolate groups, that can shift the reduction potentials to more negative values and improve solubility. However, it has been shown that the position of the phenolate groups on the aromatic ring significantly influence these two critical parameters for AORFBs [11-14]. For example, dyes with reasonable prices at tons scale such as alizarin (15-20 €/kg) and quinizarin (7-13 €/kg) exhibit water-solubility lower than 0.2 mol L^{-1} [11]. Chains with solubilizing groups have been also introduced on the aromatic backbone to improve the solubility of anthraquinones (Scheme 1) [6].

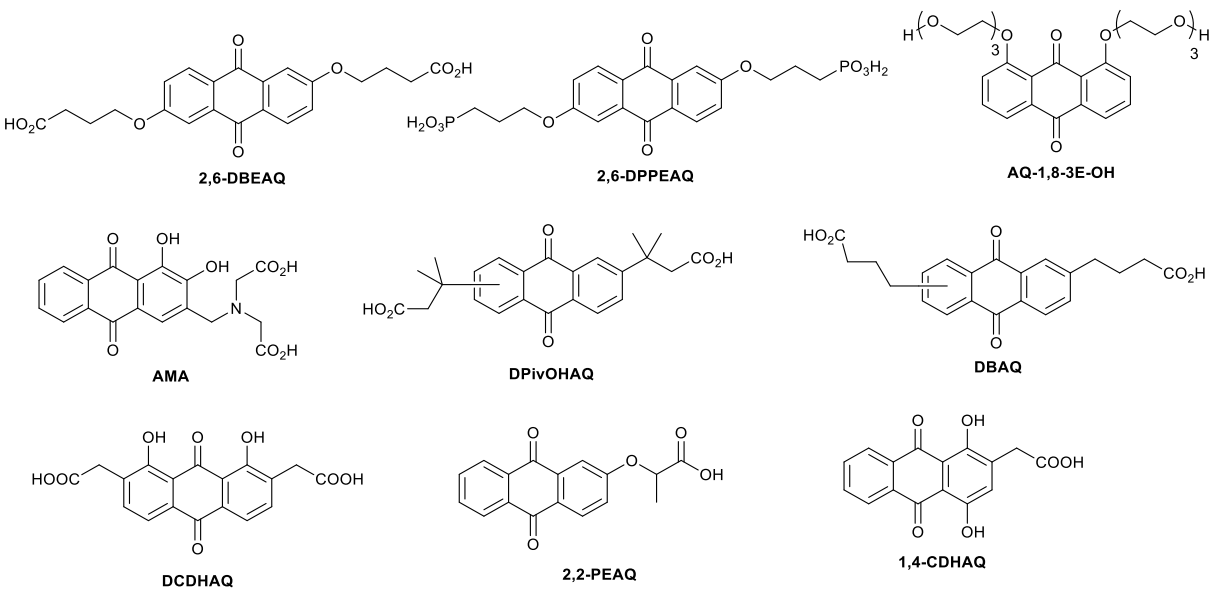

Scheme 1 Anthraquinones with solubilizing chains

O-alkylation reaction is a simple way to add side-chains on hydroxylated anthraquinones. Thus, 4,40-((9,10-anthraquinone-2,6-diyl)dioxy)dibutyrate (2,6-DBEAQ) with two carboxylic acid chains has been prepared from 2,6-dihydroxyanthraquinone. It exhibits a high solubility (0.6 mol L^{-1} at pH 12) and has demonstrated a good stability in AORFB with a capacity fade rate of

< 0.01%/day for 26 days [15]. A similar synthetic process has also led to the synthesis of (((9,10-dioxo-9,10-dihydroanthracene-2,6-diyl)bis(oxy))bis(propane-3,1-diyl))bis(phosphonic acid) (2,6-DPPEAQ) with two phosphonate chains with a solubility of 0.75 mol L^{-1} at pH 9 [16] By pairing with potassium ferri/ferrocyanide posolyte, this compound has shown high stability for 12 days with a capacity fade rate of only 0.014%/day. It is worth noting that under strong alkaline conditions, a hydroxide-mediated nucleophilic substitution reaction (SNAr or SN2) dominates in the decomposition of both 2,6-DBEAQ and 2,6-DPPEAQ and a higher stability was obtained when decreasing the pH of the electrolyte [3]. The introduction of solubilizing polyethyleneglycol (PEG) side chains onto hydroxyanthraquinones has also been performed through Williamson etherification [17]. Thus, 8-bis(2-(2-(2-hydroxyethoxy)ethoxy)-ethoxy)anthracene-9,10-dione (AQ-1,8-3E-OH) synthesized from 1,8-dihydroxyanthraquinone could be implemented in AORFBs at a concentration of 1.5 mol L^{-1} in 1 mol L^{-1} KCl with a capacity fade rate of 0.5%/day for 18 days. The authors have isolated a dimer (tetra-triethyleneglycol-substituted dianthrone) as main by-product. Indeed, the formation of anthrone has already been observed in AORFBs in acidic medium, resulting from the reduction of anthrahydroquinone [18, 19]. However it has been recently shown that this reaction is reversible when a deep discharge is applied [20]. To avoid nucleophilic substitution of OR groups, the addition of solubilizing chains via carbon-carbon bonds was also attempted. 1,4-dihydroxyanthraquinone 2,3-dimethylsulfonic acid (DHAQDMS) has been prepared by reaction of sodium sulphite on 1,4-dihydroxy-2,3-bis(bromomethyl)anthraquinone in the presence of potassium iodide [21]. However, the molecule was not stable at high state of charge when paired with bromide in acidic conditions. The synthesis of alizarin-3-methyliminodiacetic acid (AMA) has also been achieved by a Mannich condensation reaction from alizarin [22]. The compound had a solubility of 0.46 mol L^{-1} in 0.2 mol L^{-1} KOH solution and exhibited a capacity fade rate of 0.81%/day for 9 days in AORFB. More recently, anthraquinones with

dicarboxylic acid side-chains have been prepared by electrochemical oxidation of disubstituted anthracenes [23, 24]. 3,3'-(9,10-anthraquinone-diyl)bis(3-methylbutanoic acid) (DPivOHAQ) and 4,4'-(9,10-anthraquinone-diyl)dibutanoic acid (DBAQ) have been successfully implemented in redox flow battery with ferrocyanide posolyte at pH 12 and demonstrated high stability with capacity fade rates of 0.014%/day and 0.0084%/day for 32 days, respectively. High solubilities of 1 mol L^{-1} for DBAQ and 0.74 mol L^{-1} for DPivOHAQ were obtained. Furthermore, the authors reported that the formation of anthrone was responsible of the loss of stability, which can be limited at pH 14 and suggested a regeneration of the electrolyte by air exposure.

In our effort to study the performance of low-cost soluble anthraquinone derivatives in redox flow battery, we focus our attention on 1,4-dihydroxy-2-carboxymethyl-9,10-anthraquinone (1,4-CDHAQ), a quinizarin substituted by a carboxylic acid chain. In fact, such product has been described by Marschalk at the beginning of the XX^{th} century in the context of the dye industry development [25, 26]. The one-pot synthesis of this compound from low-cost commercially available leucoquinizarin made it a very good candidate for AORFBs. Meantime, the double substituted 1,8-dihydroxy-2,7-dicarboxymethyl-9,10-anthraquinone (DCDHAQ) derivative has been published by Aziz *and coll.*, which shown a solubility of 1.3 M at pH 14 and has shown a low capacity fade rate of 0.03% per day for 9 days when charging was limited to 80% state of charge (SOC) [27]. He also shown the high solubility (1.0 M) at pH 14 of (1,4-CDHAQ) but did not test it in redox flow battery due to its possible oxidation by ferricyanide. Since this degradation process is membrane and posolyte dependant, we thought that it was interesting to report its physico-chemical properties and its behaviour in redox flow battery. In this work, 1,4-CDHAQ has been studied at pH < 14 to avoid too strong basic medium that leads to the degradation of the ferri/ferrocyanide complex in the presence of dioxygen [28-30]. It was

then supplemented in a redox flow battery with ferrocyanide posolyte, paying particular attention to the link between cycling conditions and chemical stability of 1,4-CDHAQ.

2. Experimental part

2.1. General

Potassium hydroxide (85%), potassium ferrocyanide hexahydrate (96%) were purchased from VWR (US). Leucoquinizarine (> 98%) was provided by TCI chemicals and glyoxylic acid monohydrate (98%) by Sigma Aldrich. NMR deuterated solvents were purchased from Eurisotop (France). All reagents were used without further purification. All solutions were prepared with ultrapure water (18.2 MΩ, Millipore Simplicity, Millipore SAS, Molsheim, France).

^{1}H NMR spectra were recorded on BRUKER AC 300 P (300 MHz) spectrometer. Chemical shifts are expressed in parts per million downfield using residual undeuterated solvent pic for calibration (3.58 and 1.72 for THF-d_8). Data are given in the following order: δvalue, multiplicity (s, singlet; m, multiplet), number of protons. ^{13}C NMR was calibrated in same way using 67.2 and 25.3 ppm for THF-d_8.

2.2. Synthesis of 1,4-CDHAQ

Into a 2 L three necked-flask equipped with a thermometer, a bubbler, an argon balloon and a big olive shape stir bar were introduced 1 L of water degassed under argon, KOH (98.8 g, 1.5 mol), leucoquinizarine (60.5 g, 0.25 mol) and glyoxylic acid monohydrate (23.0 g, 0.25 mol). The solution was stirred at 55°C for 18 hours. After cooling to room temperature, the solution was diluted with 500 mL of water, and the pH adjusted to pH 12 using 3 M HCl solution. The solution was filtered by gravity to separate a violet-black insoluble residue. The filtrate was acidified with 3 M HCl solution to give a red-brown precipitate, filtered through a Büchner

apparatus and thoroughly washed with water (3 x 500 mL). After dispersion in water, the product was lyophilized to give a red brick light powder (70.9 g, 95 % yield) sparingly soluble in THF-d_8.

^{1}H (300 MHz, THF-d_8): 13.31 (s, 1H), 12.83 (s, 1H), 8.32 (m, 2H), 7.89 (m, 2H), 7.34 (s, 1H), 3.72 (s, 2H). Carboxylic acid proton not observable.

^{13}C (75 MHz, THF-d_8): 187.8 (C), 187.3 (C), 170.9 (C), 158.1 (C), 157.4 (C), 138.1 (C), 135.2 (CH), 135.1 (CH), 134.4 (C), 134.2 (C), 130.4 (CH), 127.4 (CH), 127.3 (CH), 112.9 (C), 112.5 (C), 35.2 (CH_2).

2.3. Solubility measurements

Oxidized form

Into 4 mL vials with teflon screw caps were introduced 298 mg (1 mmol) of 1,4-CDHAQ, 2 to 4 equivalents of NaOH or KOH using 8 M mother solutions, and water to reach 2000 µL overall volume (the mass of 1,4-CDHAQ was taken into account in the global volume and density was considered equal to 1). After 3 days equilibration in an air-conditioned room at 25 °C and using rotary agitator, the solutions were filtered through 0.2 µm cellulose acetate syringe filters, diluted sequentially by 100 and 40 folds in THF acidified with 0.1 M H_2SO_4 to record UV-vis spectra using an Agilent CARY 60 apparatus (Agilent Technologies, Santa Clara, USA). ε(0.1 M H_2SO_4 in THF, 484 nm) = 9 190 M^{-1} cm^{-1}.

Reduced form

The reduced form of 1,4-CDHAQ was prepared under argon in an AORFB operated under positive current until 100% SOC was reached. The negolyte was a 0.4 mol L^{-1} solution of 1,4-CDHAQ in a 1.4 mol L^{-1} KOH aqueous solution (25 mL) and the posolyte was a 0.4 mol L^{-1} solution of potassium ferrocyanide in a 0.2 mol L^{-1} KOH aqueous solution (50 mL). About 1

mL of negolyte was collected at the end of the charge with a cannula and water was evaporated under vacuum. Oxygen-free distilled water was added in a glovebox and after filtration on a 0.22 µm filter, the solution was diluted and left oxidized in the air to 1,4-CDHAQ. The concentration of the solution was estimated by UV-visible spectroscopy analysis on an AvaSpec-2048 spectrometer (Avantes). The absorbance spectra of 1,4-CDHAQ revealed two peaks at 561 nm and 596 nm, used to draw the calibration curves (Fig. S1). The maximum of solubility of the reduced form of 1,4-CDHAQ was estimated to be 0.77 mol L^{-1}.

2.4. Electrochemical analyses

Cyclic voltammetry analyses were carried out with a glassy carbon electrode (diameter 3 mm), a platinum wire auxiliary electrode, and an Ag/AgCl reference electrode in a bridge tube in a standard three-electrode configuration, with a SP50 (Biologic) potentiostat/galvanostat (France). The initial potential sweep was from -0.4 V to -1.5 V. Linear Sweep Voltammetry (LSV) was performed with a 0.071 cm^2 glassy carbon rotating disc electrode (Metrohm) at 20 mV s^{-1} scan rate under a nitrogen atmosphere.

2.5. AORFB experiments

The redox flow battery was composed of two graphite felt electrodes (SGL carbon SE; square cuboid 50 × 50 × 4.6 mm with a geometrical surface area of 25 cm^2; 35% compression of the thickness leading to 95.5% porosity), two composite graphite current collectors and a cationic ion-exchange membrane (50 µm Nafion membrane). The posolyte and negolyte were pumped from opaque tanks at a flow rate of 100 mL min^{-1} through KNF Pumps (Liquiport® 1.100 version KT). All battery experiments were protected from light. The battery was operated through a BT-Lab V1-57 software controlling a BioLogic Science Instruments BCS 815 (France). The cycling current was set at 40 mA cm^{-2} both in charge and discharge and voltage

cut-offs were 1.3 V in charge and between 0.3 and 0.8 V in discharge. Retention capacity was defined as the ratio between the discharge capacity for cycle n and the initial discharge capacity.

3. Results and discussion

3.1. Physico-chemical properties of 1,4-CDHAQ

The solubility of 1,4-CDHAQ was tested with different equivalents of KOH and NaOH (Fig. 1). The initial concentration of anthraquinone was fixed at 0.5 M since first tests performed at pH 13 showed the presence of solid at this concentration. The solubility of 1,4-CDHAQ increased with the pH up to 14 with a value ≥ 0.5 M, which is consistent with previously reported results [27]. At pH 13 chosen in this study, the solubility was around 0.4 M, corresponding to a theoretical volumetric capacity of 27 A h L^{-1}.

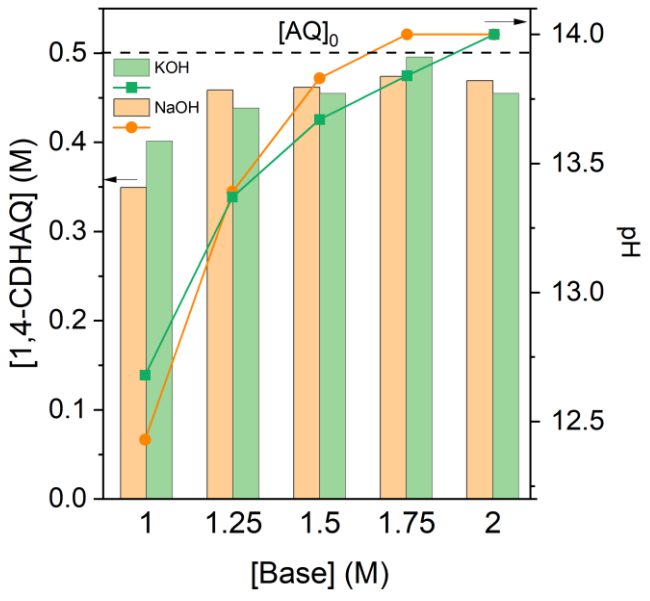

Fig. 1. Maximum solubility of 1,4-CDHAQ and measured pH *versus* the concentration of KOH and NaOH estimated from UV measurement after filtration of a 0.5 M 1,4-CDHAQ.

The solubility of the reduced form of 1,4-CDHAQ was estimated at 0.77 M at a pH around 13.5, which underlines that it is not a limiting parameter.

Cyclic voltammetry in 0.1 M KOH showed a quasi-reversible system at -0.72 V *vs*. Ag/AgCl (Fig. 2a). If used in redox flow battery with ferri/ferrocyanide as posolyte at pH 13, an open-circuit voltage around 1 V will be obtained at 50% SOC. When the potential was increased, an irreversible wave was observed with an onset around 0.1 V vs Ag/AgCl, leading to the appearance of a peak at -0.61 V *vs* Ag/AgCl (Fig. 2b). A good control of the discharge potential will therefore be necessary to avoid the degradation of 1,4-CDHAQ by oxidation during cycling in RFB. The Pourbaix diagram shown in Fig. 2c exhibited a straight line between pH 12.4 and 14, with a slope of -31.1 mV pH^{-1}, corresponding to a 1-proton/2-electron process. This behavior is consistent with those of DCDHAQ [27] and underlines that increasing the pH will increase the cell potential. The diffusion coefficient of 1,4-CDHAQ was determined by rotating disk electrode analyses from the Levich equation to be 2.5×10^{-6} cm^2 s^{-1} (Fig. S2a) and the electron transfer rate constant k^0 was estimated as 9.6×10^{-4} cm s^{-1} from the Tafel plot (Fig. S2b and c). These values are slightly higher than those reported for DCDHAQ (1.7×10^{-6} cm^2 s^{-1} and 7.4×10^{-4} cm s^{-1}, respectively) [27].

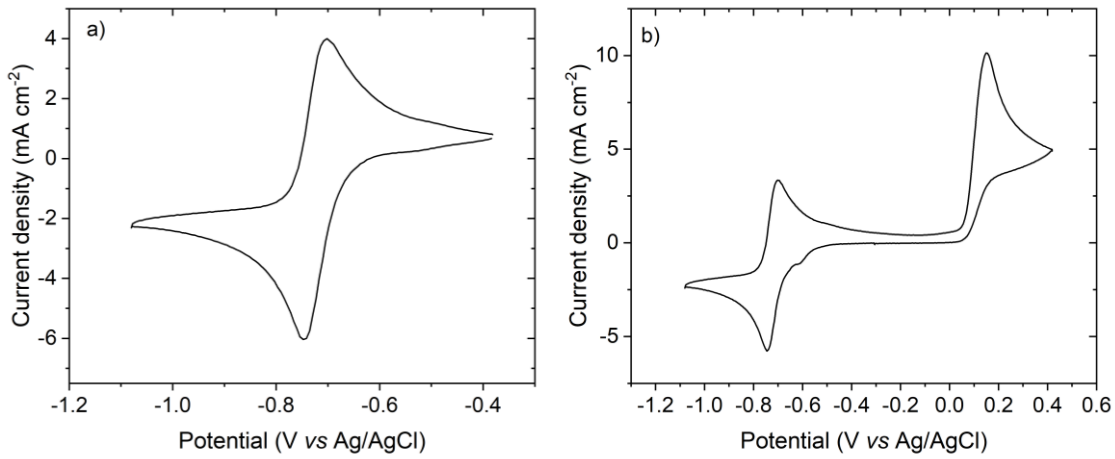

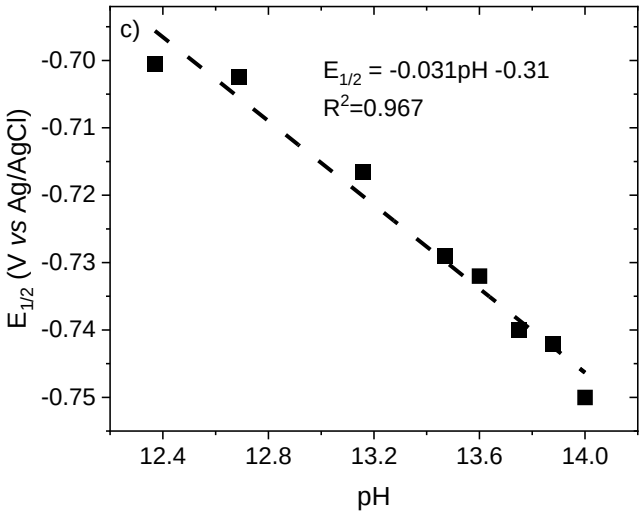

Fig. 2. Cyclic voltammogram of 5 × 10^{-3} M 1,4-CDHAQ in 0.1 M KOH on glassy carbon electrode with Emax = -0.40 V *vs* Ag/AgCl (a) and 0.4 V *vs* Ag/AgCl (2^{nd} cycle) (b). 100 mV s^{-1}. c) Pourbaix diagram of 1,4-CDHAQ (Redox potential *vs* pH).

3.2. Performance of 1,4-CDHAQ in AORFBs

The electrochemical performances of the AORFB cell based on 0.4 M 1,4-CDHAQ and 0.4 M ferrocyanide redox pairs at pH 13 were evaluated at room temperature. The cell was galvanostatically charged at 1.3 V and discharged at 0.3 V. Typical charge−discharge plots were measured with a current density of 40 mA cm^{-2} (Fig. 3).

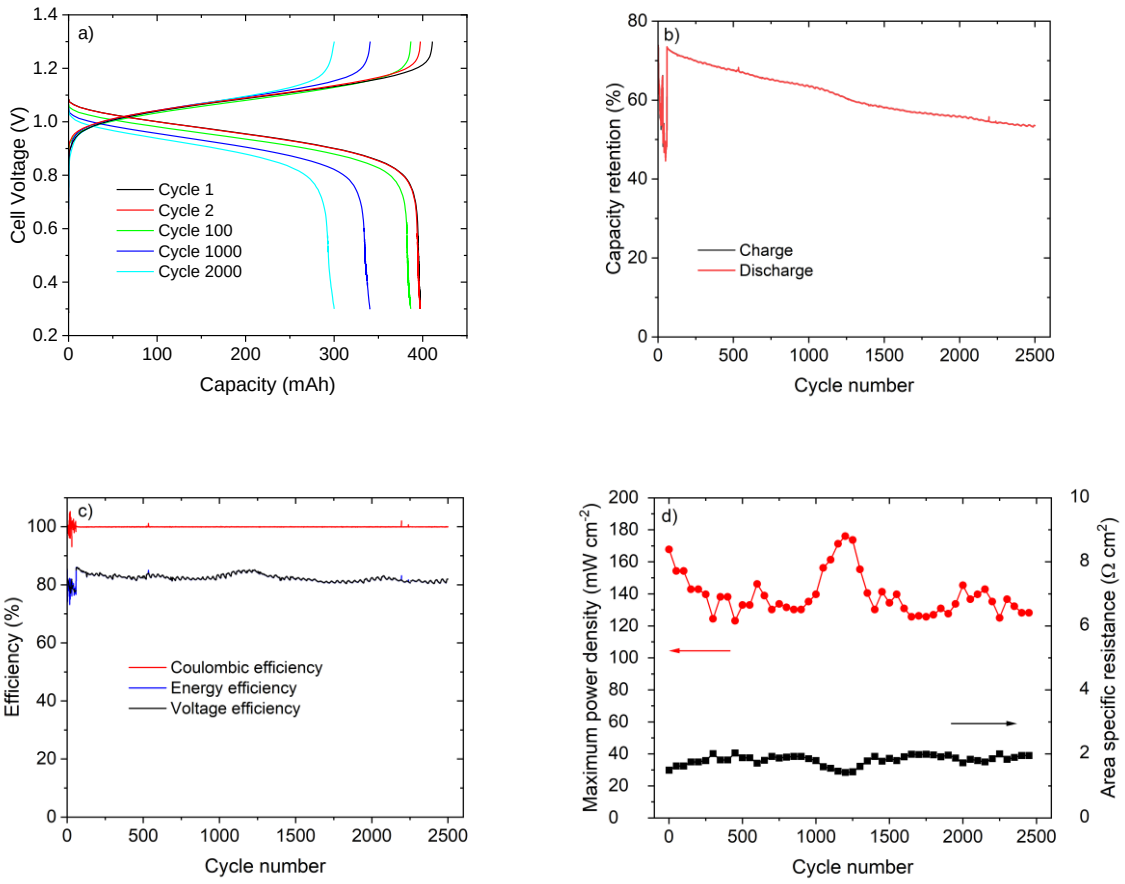

Fig. 3. a) Charge-discharge curves for different cycles and b) evolution of the capacity retention with the cycle number for 0.4 M $K_4[Fe(CN)_6]$ in 0.2 M KOH posolyte (50 mL) and 0.4 M 1,4-CDHAQ in 1.4 M KOH negolyte (25 mL) (40 mA cm^{-2}; cut-off voltages 1.3 V and 0.3 V) for 72 days c) Coulombic efficiency, voltage efficiency and round-trip energy efficiency d) Maximum power density at a 50% state of charge (SOC) and cell resistance *vs* number of cycles.

In these conditions of charge, the initial capacity was only 74% of the theoretical one. It could be improved with a limited risk of hydrogen evolution if a potentiostatic charge step at 1.3 V was applied. The capacity slowly decreased with the number of cycles with a significant drop between cycles 4 and 24 due to unintentional pump stops. A total capacity fade rate of 0.008%/cycle (0.28%/day) was measured on this long-cycling experiment.

The coulombic efficiency was close to 100%, as observed with other anthraquinone derivatives [12, 27] and the energy efficiency around 82% was significantly higher than the value reported for DCDHAQ (~ 60%), which is probably due to a higher resistance in the system. The area specific resistance varies between 1.5 and 2 Ω cm^2 (Fig. 3d), which is acceptable for AORFB application. The maximum power density P_{max} at 50% SOC was estimated from the area specific resistance, considering the optimum of the following equation:

$$P = E_{cell}I - RI^2$$

It led to:

$\frac{dP}{dI} = E_{cell} - 2RI = 0$ and $Pmax = \frac{Ecell^2}{4R}$

With E_{cell}, the value at 50% of SOC (around 1V), I, the current and R the area specific resistance.

The value decreased from 170 to 135-140 mW cm^{-2}, due to the increase of the resistance during the first 100 cycles. Excluding cycles between 1000 and 1400 for which a variation of the resistance occurs probably due to higher room temperature, it was quite stable during the long-cycling AORFB.

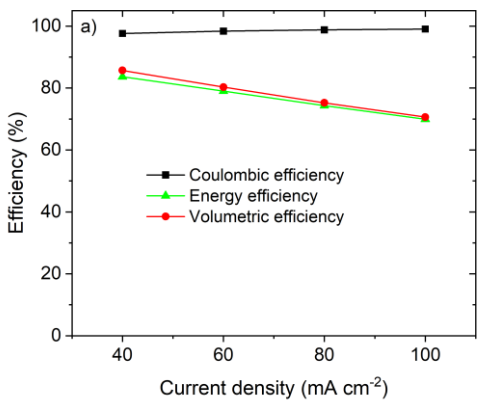

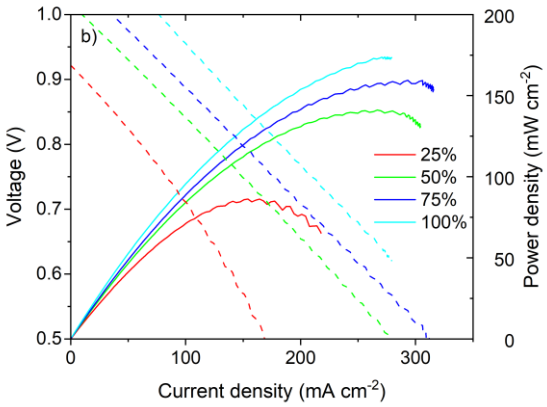

Fig. 4. Cycling performances of the 1,4-CDHAQ/$K_4Fe(CN)_6$ AORFBs at high concentration. The electrolytes were 25 mL of 0.4 M 1,4-CDHAQ in 1.4 M KOH (negolyte) and 50 mL of 0.2 M $K_4Fe(CN)_6$ in 0.2 M KOH (posolyte). (a) Coulombic efficiency, energy efficiency, and capacity utilization of the cell at different current densities. (b) Power density *versus* current density at 25, 50, 75 and 100% SOC.

Investigations of the battery performance at various current densities ranging from 20 to 100 mA cm^{-2} were conducted (Fig. 4). The 1,4-CDHAQ/$K_4Fe(CN)_6$ cell exhibited an excellent rate performance without large capacity loss and with a coulombic efficiency always above 97% and a peak efficiency of 84% at a current density of 40 mA cm^{-2}. The energy efficiency displayed a linear relationship with current density, showing an almost constant battery resistance and volts-ampere characteristics.

The polarization curves (Fig. 4c) were performed at 25, 50, 75 and 100% state of charge. A peak galvanic power density of 170 mW cm^{-2} was obtained at 100% SOC, which is close to the value of 160 mW cm^{-2} previously obtained with DCDHAQ [27]. A value of 140 mW cm^{-2} was measured at 50% SOC, which is in the range of the values previously estimated during the long-cycling AORFB, especially as no pre-treatment was performed on the membrane and graphite felt electrodes.

For a better understanding of the effect of the cut-off voltage in discharge on the capacity fade rate of the battery, different values were fixed and the anthraquinone degradation was checked by NMR analysis. The capacity fade rate estimated after 300 cycles for three batteries performed in the same conditions except the cut-off voltage fixed at 0.3, 0.6 and 0.8 V is given in Table 1.

Table 1
Effect of the Cut-off voltage on the capacity fade rate over 300 cycles.

Cut-off voltage in discharge (V)	Capacity fade rate	
	%/cycle	%/day
0.3	0.016	0.43
0.6	0.012	0.32
0.8	0.013	0.35

Although the stability and the performance were similar for batteries performed with a cut-off voltage of 0.6 and 0.8 V (Fig. S4), a slightly higher degradation was observed when the value was fixed at 0.3 V. ^{1}H-NMR analysis of the negolyte was performed after 1300 and 2500 cycles (Fig. 5 and Fig. S3). New peaks between 7.8 and 8 ppm and 7.3 and 7.6 ppm appeared and increased with the RFB cycling (Fig. S3), showing the formation of degradation products. Since 1,4-CDHAQ exhibited an irreversible oxidation wave in cyclic voltammetry with an onset around -0.1 V *vs.* Ag/AgCl, a possible degradation pathway would be its oxidation during battery operation. The crossover of Fe(III) species through the membrane is unlikely considering the high amount of formed by-products and other long-cycling experiments performed in similar conditions in our laboratory [12, 13]. A possible explanation would be the low cut-off voltage during discharge allowing the negolyte compartment to reach the oxidation potential of 1,4-CDHAQ, especially if we consider the inhomogeneous flow repartition in the porous electrode. This hypothesis was confirmed by the ^{1}H-NMR analysis of 1,4-CDHAQ performed in the presence of ferricyanide (Fig. 5). Indeed, new peaks, similar to those observed after 2500 cycles, were observed. The negolyte solutions of the two other batteries performed with cut-off voltages in discharge of 0.6 and 0.8 V were also analyzed by ^{1}H-NMR (Fig. 6).

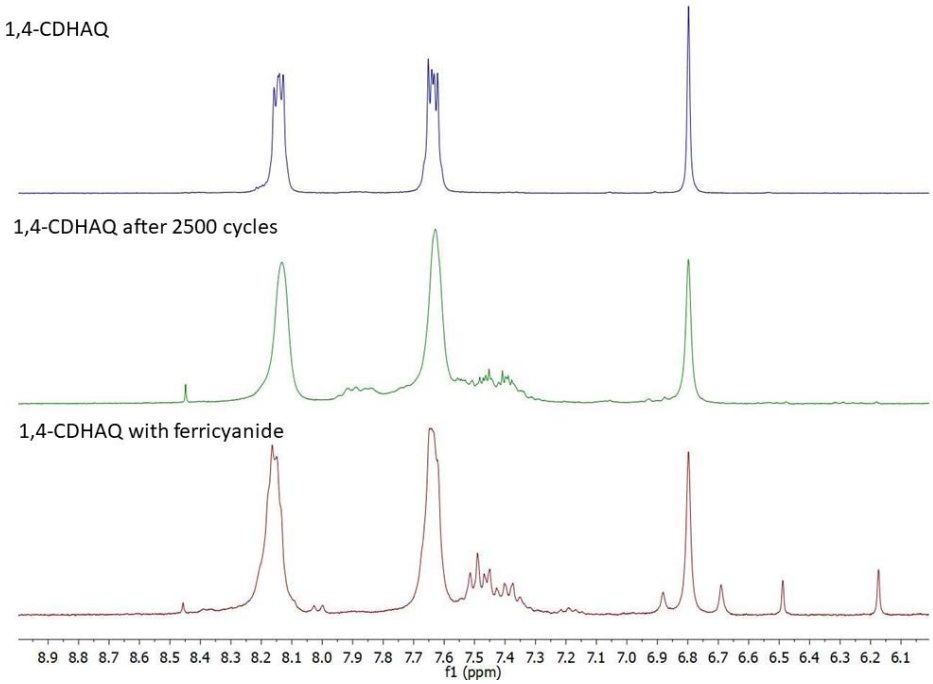

Fig. 5. ^{1}H-NMR in D_2O of 1,4-CDHAQ before (blue) and after (green) AORFB cycling (2500 cycles) and after addition of potassium ferricyanide (red).

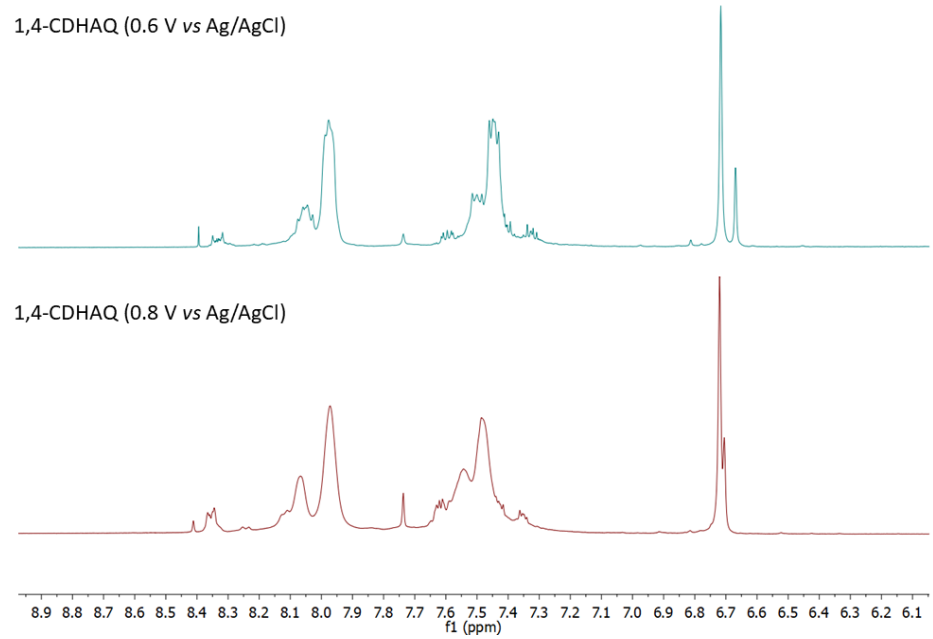

Fig. 6. ^{1}H-NMR in D_2O of 1,4-CDHAQ after AORFB cycling with a cut-off voltage of 0.6 V (blue) and 0.8 V (red).

Although the capacity fade rates obtained for these batteries were slightly lower, ^{1}H-NMR revealed the formation of new products. A slight shift of the peaks was observed probably due to the evolution of the electrolytic medium during cycling. The integration of the aromatic peaks (Fig. S4) showed new peaks close to the AB system of 1,4-CDHAQ and a new singlet around 6.7 ppm, which could be attributed to another compound with a similar molecular structure. The formation of anthrone has been reported in alkaline medium, resulting from a disproportionation reaction of anthrahydroquinone derivatives and/or from their electrochemical reduction [31, 32]. The authors claimed that anthrone can either be readily oxidized into dianthrone, which further decomposed into other by-products, or can be oxidized back into anthraquinone by dioxygen. Although the identification of the formed compounds was not the purpose of this study and would require further analyses in operando, this degradation pathway could explain the apparition of a new aromatic peaks, even if hydroxyl substituents close to the carbonyl groups have been reported to limit the formation of anthrone for 1,5-dihydroxyanthraquinone compared with 2,6-dihydroxyanthraquinone [33]. The presence of small peaks between 7.3 and 7.4 cannot rule out the hypothesis of 1,4-CDHAQ oxidation. Interestingly, the new aromatic peaks were not observed when a low cut-off voltage of 0.3 V was used (Fig. 5). This could be explained by the reoxidation of anthrone into the initial anthraquinone during the low discharge step, as previously reported before [13, 34].

The effect of temperature on ASR was evaluated by cycling a solution of 0.4 M 1,4-CDHAQ as negolyte and 0.4 M ferrocyanide as posolyte at pH 13 in a thermostat cabinet. The cell was galvanostatically charged at 1.3 V and discharged at 0.45 V to minimize both the oxidation of 1,4-CDHAQ and anthrone formation. A temperature of 30°C was used for the first 20 cycles and then decreased in 5°C steps to 15°C and finally increased back to 30°C. The evolution of the capacity retention and ASR with the number of cycles is given in Fig. 7.

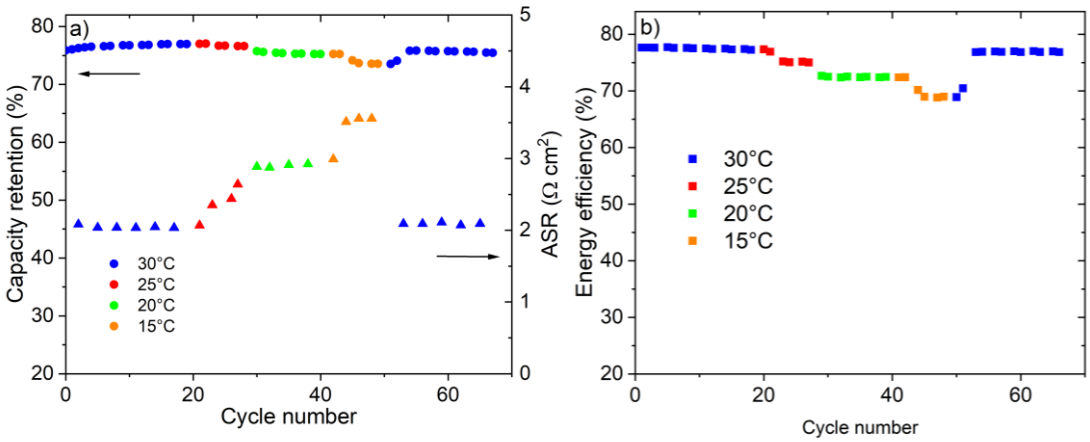

Fig. 7. Evolution of the a) capacity retention, ASR and b) energy efficiency with the cycle number and the temperature for 0.4 M $K_4[Fe(CN)_6]$ in 0.2 M KOH posolyte (50 mL) and 0.4 M 1,4-CDHAQ in 1.4 M KOH negolyte (25 mL) (40 mA cm^{-2}; cut-off voltages 1.3 V and 0.45 V).

As expected, the accessible capacity slightly decreased with the temperature due to a decrease of the electron-transfer kinetics. The variation of ASR with temperature is high (around 0.1 Ω cm^2 / °C), affecting the power density of the battery and its energy efficiency. Initial values of ASR, capacity and energy density were recovered when the temperature was increased from 15°C to 30°C, showing the good stability of the battery in these cycling conditions.

Table 2 summarizes the performance of long cycling of substituted anthraquinones in AORFB. Considering that the experiments were not carried out in a glovebox, the fade rate of 1,4-CDHAQ (0.28%/day) is close to other anthraquinones used at pH ≥ 13: higher than AQ-1,8-3E-OH, similar to AMA and 4-5 times higher than DCDHAQ and 2,2-PEAQ. Only DPivOHAQ has a significantly higher stability in strong basic medium.

Table 2
Reported performances for long cycling in AORFBs of anthraquinones substituted by solubilizing chains with ferri/ferrocyanide as posolyte.

Redox species	Initial pH	Concentration for long cycling (mol L^{-1})	Number of cycles	Fade rate (%/day) (number of days)	Energy efficiency (%) (current density mA cm^{-2})	Max. power density at 50% SOC (W cm^{-2})	Ref.
2,6-DBEAQ	12	0.5	350	0.04 (6)	85 (50)	0.19	[15]
2,6-DPPEAQ	9-13	0.5	480	0.014 (12)	65 (100)	0.13	[16]
AQ-1,8-3E-OH	7-12.8	1.5	220	0.5 (18)	75 (50)	0.12	[17]
AMA	13.3	0.4	350	0.19 (9)	90 (50)	0.29	[22]
DPivOHAQ	12	0.5	690	0.014 (15.6)	92 (50)	0.3	[23, 24]
	14	0.5	690	0.0018 (16)	-	-	
DBAQ	12	0.5	650	0.0084 (15.5)	-	-	[23]
DCDHAQ	14	0.2	1422	0.068 (23)	-	-	[27]
		0.75	93	0.03 (9)	60-63 (40)	0.14	
2,2-PEAQ	7	0.1	2000	0.09 (10)	69 (40)	0.87	[35]
	14	0.1	850	0.05 (10)			
1,4-CDHAQ	13	0.4	2500	0.28 (72)	84 (40)	0.17	This work
			1500	0.27 (53)			

4. Conclusions

In summary, the low-cost anthraquinone 1,4-CDHAQ exhibited good performance in AORFB. It has high solubility (> 0.4 M) in strong basic medium and pairing with potassium ferri/ferrocyanide posolyte, a cell voltage of about 1V. Cycling experiments performed with a galvanostatic charge led to an initial capacity of only 70-80% of the theoretical one, although a potentiostatic charge step was not tested. Although the coulombic efficiency (close to 100%) was similar to DCDHAQ, the energy efficiency (82%) and the power density at 100% SOC (170 mV cm^{-2}) were higher (~60%; 160 mV cm^{-2}). The variation of temperature strongly influenced the ASR and so did the power density, showing the importance to control the temperature for reproducible and accurate measurements. The long cycling of 0.4 M 1,4-CDHAQ carried out over 72 days showed a total capacity fade rate of 0.008%/cycle (0.28%/day). These results are similar to other capacity fade rate reported for long-cycling of anthraquinone derivatives in AORFB at pH ≥ 13. A significant effect of the discharge cut-off voltage on the nature of degradation products was highlighted with the oxidation of the

anthraquinone when a low cut-off voltage (0.3 V) was applied. These results highlighted the importance of the cycling conditions for stability enhancement of anthraquinone derivatives.

Author contributions

I. Ozouf: Investigation, Validation, Formal analysis, Conceptualization. J.-M. Fontmorin: Investigation, Validation, Formal analysis, Review. R. Lebeuf: Investigation, Validation, Formal analysis, Visualization, Funding acquisition, Writing - Review. G. Mathieu: Investigation, Formal analysis. S. Guiheneuf: Investigation, Formal analysis, Review. G. Ozouf: Conceptualization. T. Godet-Bar: Project administration, Funding acquisition, Review. D. Floner: Conceptualization, Project administration, Funding acquisition, Review. J.-M. Aubry: Supervision, Project administration, Funding acquisition, Review. F. Geneste: Writing - Review & Editing, Visualization, Supervision, Project administration, Funding acquisition.

Acknowledgements

This work was supported by the French National Agency (ANR-19-CE05-0012, Programme AAPG 2019) and the CNRS Energy unit (PEPS Cellule Energie 2021).

References

[1] R. Chen, Redox flow batteries for energy storage: Recent advances in using organic active materials, Curr. Opin. Electrochem., 21 (2020) 40-45.

[2] Y. Liu, Q. Chen, P. Sun, Y. Li, Z. Yang, T. Xu, Organic electrolytes for aqueous organic flow batteries, Mater. Today Energy, 20 (2021) 100634.

[3] J. Luo, B. Hu, M. Hu, Y. Zhao, T.L. Liu, Status and Prospects of Organic Redox Flow Batteries toward Sustainable Energy Storage, ACS Energy Lett., 4 (2019) 2220-2240.

[4] V. Singh, S. Kim, J. Kang, H.R. Byon, Aqueous organic redox flow batteries, Nano Res., 12 (2019) 1988-2001.

[5] F. Zhong, M. Yang, M. Ding, C. Jia, Organic electroactive molecule-based electrolytes for redox flow batteries: status and challenges of molecular design, Front. Chem., 8 (2020) 00451.

[6] P. Symons, Quinones for redox flow batteries, Curr. Opin. Electrochem., 29 (2021) 100759.

[7] J.-M. Fontmorin, S. Guiheneuf, T. Godet-Bar, D. Floner, F. Geneste, How anthraquinones can enable aqueous organic redox flow batteries to meet the needs of industrialization, Curr. Opin. Colloid Interface Sci., 61 (2022) 101624.

[8] K. Lin, Q. Chen, M.R. Gerhardt, L. Tong, S.B. Kim, L. Eisenach, A.W. Valle, D. Hardee, R.G. Gordon, M.J. Aziz, M.P. Marshak, Alkaline quinone flow battery, Science, 349 (2015) 1529-1532.

[9] A. Le, D. Floner, T. Roisnel, O. Cador, L. Chancelier, F. Geneste, Highly soluble Fe(III)-triethanolamine complex relevant for redox flow batteries, Electrochim. Acta, 301 (2019) 472-477.

[10] J.-M. Fontmorin, S. Guiheneuf, P. Bassil, F. Geneste, D. Floner, Addition of weak acids in electrolytes to prevent osmosis in aqueous organic redox flow batteries, Electrochem. Commun., 132 (2021) 107148.

[11] K. Wedege, E. Drazevic, D. Konya, A. Bentien, Organic Redox Species in Aqueous Flow Batteries: Redox Potentials, Chemical Stability and Solubility, Sci. Rep., 6 (2016) 39101.

[12] S. Guiheneuf, A. Le, T. Godet-Bar, L. Chancelier, J.-M. Fontmorin, D. Floner, F. Geneste, Behaviour of 3,4-Dihydroxy-9,10-Anthraquinone-2-Sulfonic Acid in Alkaline Medium: Towards a Long-Cycling Aqueous Organic Redox Flow Battery, ChemElectroChem, 8 (2021) 2526-2533.

[13] S. Guiheneuf, T. Godet-Bar, J.-M. Fontmorin, Jourdin C., D. Floner, F. Geneste, A new hydroxyanthraquinone derivative with a low and reversible capacity fading process as negolyte in alkaline aqueous redox flow batteries, J. Power Sources, 539 (2022) 231600.

[14] T. Gaudin, J.-M. Aubry, Prediction of Pourbaix diagrams of quinones for redox flow battery by COSMO-RS, Journal of energy storage, 49 (2022) 104152.

[15] D.G. Kwabi, K. Lin, Y. Ji, E.F. Kerr, M.-A. Goulet, D. De Porcellinis, D.P. Tabor, D.A. Pollack, A. Aspuru-Guzik, R.G. Gordon, M.J. Aziz, Alkaline Quinone Flow Battery with Long Lifetime at pH 12, Joule, 2 (2018) 1894-1906.

[16] Y. Ji, M.-A. Goulet, D.A. Pollack, D.G. Kwabi, S. Jin, D. De Porcellinis, E.F. Kerr, R.G. Gordon, M.J. Aziz, A Phosphonate-Functionalized Quinone Redox Flow Battery at Near-Neutral pH with Record Capacity Retention Rate, Adv. Eng. Mater., 9 (2019) 1900039.

[17] S. Jin, Y. Jing, D.G. Kwabi, Y. Ji, L. Tong, D. De Porcellinis, M.-A. Goulet, D.A. Pollack, R.G. Gordon, M.J. Aziz, A Water-Miscible Quinone Flow Battery with High Volumetric Capacity and Energy Density, ACS Energy Lett., 4 (2019) 1342-1348.

[18] D.G. Kwabi, Y. Ji, M.J. Aziz, Electrolyte Lifetime in Aqueous Organic Redox Flow Batteries: A Critical Review, Chem. Rev., 120 (2020) 6467-6489.

[19] S. Gentil, D. Reynard, H.H. Girault, Aqueous organic and redox-mediated redox flow batteries: a review, Curr. Opin. Electrochem., 21 (2020) 7-13.

[20] Y. Jing, E.W. Zhao, M.-A. Goulet, M. Bahari, E.M. Fell, S. Jin, A. Davoodi, E. Jonsson, M. Wu, C.P. Grey, R.G. Gordon, M.J. Aziz, In situ electrochemical recomposition of decomposed redox-active species in aqueous organic flow batteries, Nat. Chem., 14 (2022) 1103-1109.

[21] M.R. Gerhardt, L. Tong, R. Gomez-Bombarelli, Q. Chen, M.P. Marshak, C.J. Galvin, A. Aspuru-Guzik, R.G. Gordon, M.J. Aziz, Anthraquinone Derivatives in Aqueous Flow Batteries, Adv. Eng. Mater., 7 (2017) 1601488.

[22] Y. Liu, S. Lu, S. Chen, H. Wang, J. Zhang, Y. Xiang, A Sustainable Redox Flow Battery with Alizarin-Based Aqueous Organic Electrolyte, ACS Appl. Energy Mater., 2 (2019) 2469-2474.

[23] M. Wu, Y. Jing, A.A. Wong, E.M. Fell, S. Jin, Z. Tang, R.G. Gordon, M.J. Aziz, Extremely Stable Anthraquinone Negolytes Synthesized from Common Precursors, Chem, 6 (2020) 1432-1442.

[24] Y. Jing, M. Wu, A.A. Wong, E.M. Fell, S. Jin, D.A. Pollack, E.F. Kerr, R.G. Gordon, M.J. Aziz, In situ electrosynthesis of anthraquinone electrolytes in aqueous flow batteries, Green Chem., 22 (2020) 6084-6092.

[25] C. Marschalk, F. Koenig, N. Ouroussoff, New method of introducing side chains into the anthraquinone nucleus, Bull. Soc. Chim. Fr., Mem., 3 (1936) 1545-1575.

[26] Compagnie nationale de matieres colorantes et manufactures de produits chimiques du Nord reunies, etablissements Kuhlmann, FR, 1933, pp. Addn to Fr 739,596 (C A 727, 2312). Compagnie nationale de matieres colorantes et manufactures de produits chimiques du Nord reunies, etablissements Kuhlmann, FR, 1933, pp. Addn to Fr 739,596 (C A 727, 2312).

[27] M. Wu, M. Bahari, E.M. Fell, R.G. Gordon, M.J. Aziz, High-performance anthraquinone with potentially low cost for aqueous redox flow batteries, J. Mater. Chem. A, 9 (2021) 26709-26716.

[28] T. Paez, A. Martinez-Cuezva, J. Palma, E. Ventosa, Revisiting the cycling stability of ferrocyanide in alkaline media for redox flow batteries, J. Power Sources, 471 (2020) 228453.

[29] J. Luo, A. Sam, B. Hu, C. De Bruler, X. Wei, W. Wang, T.L. Liu, Unraveling pH dependent cycling stability of ferricyanide/ferrocyanide in redox flow batteries, Nano Energy, 42 (2017) 215-221.

[30] M. Hu, A.P. Wang, J. Luo, Q. Wei, T.L. Liu, Cycling performance and mechanistic insights of ferricyanide electrolytes in alkaline redox flow batteries, Adv. Energy Mater., 13 (2023) 2203762.

[31] M.-A. Goulet, L. Tong, D.A. Pollack, D.P. Tabor, S.A. Odom, A. Aspuru-Guzik, E.E. Kwan, R.G. Gordon, M.J. Aziz, Extending the Lifetime of Organic Flow Batteries via Redox State Management, J. Am. Chem. Soc., 141 (2019) 8014-8019.

[32] E.W. Zhao, T. Liu, E. Jonsson, J. Lee, I. Temprano, R.B. Jethwa, A. Wang, H. Smith, J. Carretero-Gonzalez, Q. Song, C.P. Grey, In situ NMR metrology reveals reaction mechanisms in redox flow batteries, Nature, 579 (2020) 224-228.

[33] S. Huang, H. Zhang, M. Salla, J. Zhuang, Y. Zhi, X. Wang, Q. Wang, Molecular engineering of dihydroxyanthraquinone-based electrolytes for high-capacity aqueous organic redox flow batteries, Nat. Commun., 13 (2022) 4746.

[34] Y. Jing, E.W. Zhao, M.-A. Goulet, M. Bahari, E.M. Fell, S. Jin, A. Davoodi, E. Jónsson, M. Wu, C.P. Grey, R.G. Gordon, M.J. Aziz, In situ electrochemical recomposition of decomposed redox-active species in aqueous organic flow batteries, Nat. Chem., 14 (2022) 1103-1109.

[35] K. Amini, E.F. Kerr, T.Y. George, A.M. Alfaraidi, Y. Jing, T. Tsukamoto, R.G. Gordon, M.J. Aziz, An Extremely Stable, Highly Soluble Monosubstituted Anthraquinone for Aqueous Redox Flow Batteries, Adv. Funct. Mater., 33 (2023) 2211338.